Hydrated Electron Production by Reaction of Hydrogen Atoms with Hydroxide Ions: A First-Principles Molecular Dynamics Study

Jean Philippe Renault,*,† Rodolphe Vuilleumier,‡ and Stanislas Pommeret†

CEA/Saclay, DSM/IRAMIS/SCM URA-331 CNRS, F-91191 Gif-sur-Yvette Cedex, France, (CEA), and LPTMC, Universitè Pierre et Marie Curie, Tour 24, Boîte 121, 4, Place Jussieu, 75252 Paris Cedex 05, France, (LPTMC)

Received: January 11, 2008; Revised Manuscript Received: February 27, 2008

The solvated electron production by reaction between the H atom and the hydroxide anion was studied using Density Functional Theory based first-principles molecular dynamics. The simulation reveals a complex mechanism, controlled by proton transfers in the coordination sphere of the hydroxide and by the diffusion of the H atom in its solvent cavity. We formulate the hypothesis, based on a coupling between classical and first-principles molecular dynamics, that these two processes give rise to a lag time for the reaction that would explain the H atom extremely small reactivity compared to other radical species. Furthermore, the reaction observed gives an original insight in excess electron solvation.

Introduction

Elementary radical reactions in liquid water are of primary importance for the understanding of the chemical processes induced by ionizing radiation such as the production of hydrogen in nuclear waste storage[1] and radiobiology[2] but also in a variety of processes as diverse as heterogeneous catalysis[3] and oxidative stress in life sciences.[4] Although it is well-known that those primary reactions are involved in all those processes, little is known on their outcome; one reason for this is that water plays both the role of solvent and the reactant in those reactions.

Among radiolytic species, the H atom has surprisingly diverse chemical properties. It acts as a reducer with most metallic cations. However, in some cases, such as in its reaction with iron(II), it is an oxidant.[5] Like the $HO^{\bullet}$ radical, it can abstract H atoms or add to a double bond. Finally, in addition to HO^-, it can also react with weaker bases such as NH_3,[6] N_3^-,[7,8] Br^-, and I^-.[9–11] Many $H^{\bullet}$ reactions are not diffusion limited and, with kinetic constants in the 10^{-7} to 10^{-8} mol^{-1} s^{-1} range, they are among the slowest observed for radiolytic species.

In the present paper we theoretically study the reaction between the hydroxide anion (OH^-) and the $H^{\bullet}$ atom that results in the chemical production of the hydrated electron (reaction A).

$$H^{\bullet} + OH^- \xrightarrow[H_2O]{} e^-_{hyd} + H_2O \qquad (A)$$

That peculiar reaction, which is suspected to play a crucial role in the radiolysis of water at high temperature and, in particular, in the supercritical regime,[12] has been extensively studied as a prototype study of $H^{\bullet}$ reactivity.[13–16]

Two possible mechanisms have been proposed in the literature for reaction A as showed in Figure 1. The first is based on the reductive character of $H^{\bullet}$ and involves the formation of a reduced water molecule followed by the release of the excess charge to the solvent to produce the hydrated electron.[17] Nevertheless, it is difficult to define what would be the limiting step of such a reaction and what the nature of a H_2O^- would be. The second assumes that $H^{\bullet}$ is a Bronsted acid and proposes a simple proton transfer from the H atom to HO^-, acting as a base.[14] From the temperature dependence of the kinetics, the presence of an intermediate state can not be excluded,[16] but the experimental and theoretical data available so far can not definitively decide the right mechanism.

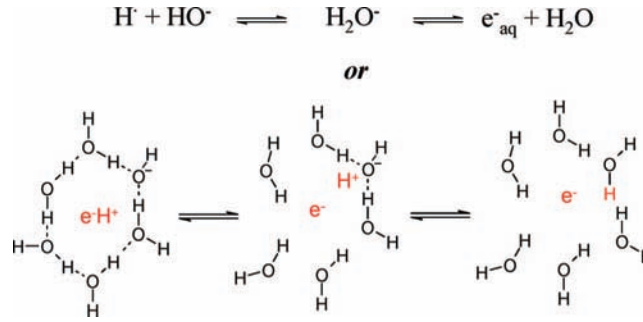

Figure 1. Possible mechanism for the chemical production of the hydrated electron. The upper one involves a temporary electron attachment to a water molecule followed by a solvation process, whereas the second one involves an electron detachment from the H atom followed by an acid−base recombination.

First-principles molecular dynamics should be well suited to tackle this problem from the theoretical side; it allows, at the same time, for an explicit description of the electrons through density functional theory (DFT), which is crucial for treating such radical reactions and for taking into account the solvent at finite temperature. As it will be seen, the solvent here plays an important role during the reaction. Recently, DFT based first-principles molecular dynamics (FPMD) has been applied to the study of the solvation of radicals in water[18] and to the study of the radical production in water during radiolytic process.[19] Of particular interest to us, FPMD has then been shown to provide a reliable description of the solvation of the hydrogen atom in water[20] and, more recently, of the solvated electron.[21–24] However, the description of the hydroxide anion by FPMD has

* Corresponding author. Fax: (+33) 1 69 08 34 66; e-mail:jprenault@cea.fr.
† CNRS.
‡ LPTMC.

10.1021/jp800269s CCC: $40.75
Published on Web 07/02/2008

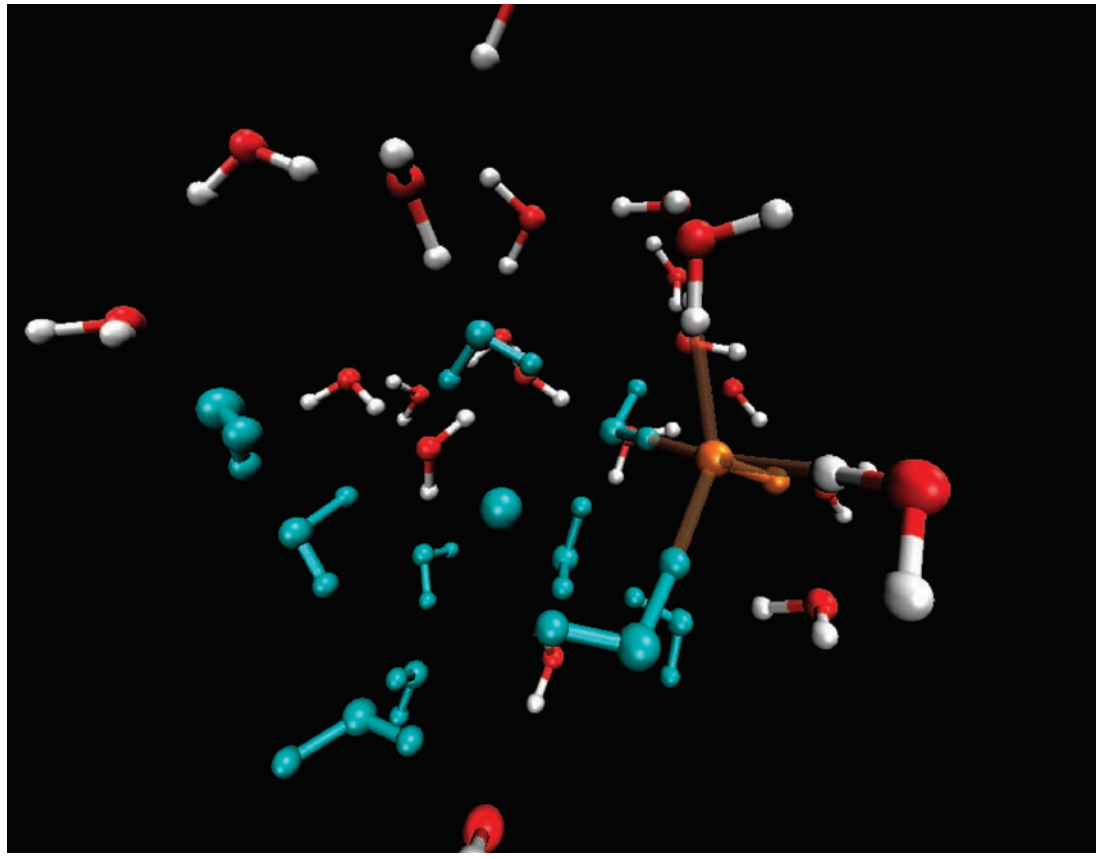

Figure 2. Metastable configuration of an encounter pair of the hydroxide anion and the H• atom in liquid water. The hydroxide anion and the four H bonds are drawn in orange. The water molecules in the first solvation shell of the H atom are drawn in grey. The water molecules in the first solvation shell of the H atom are drawn in grey. The lifetime of such configurations is on the order of a few hundreds of femtoseconds.

for some time been the subject of some controversy.[25,26] Nevertheless, proper choice of the exchange-correlation functional leads to the correct description of the OH^- solvation and diffusion mechanism.[26]

The objective of the present paper is to propose a mechanism for reaction A based on the results of FPMD.

Numerical Methods

Initial atomic configurations were obtained from classical molecular dynamics simulations employing an SPC/E potential for the water−water interaction.[27] The HO^- description was obtained from ref 28 and is known to adequately describe the hydroxide diffusion in water. The parameters for the free H atom were adapted from the Lennard−Jones parameters given in ref 29. Constant-volume FPMD simulations in spin density functional theory framework were performed using the Car−Parrinello molecular dynamics (CPMD) method[30,31] with a fictitious mass of 700 au for the electron and an integration time step of 0.1209 fs. The spin dependent one-electron orbitals are expanded in a plane wave basis set, with a kinetic energy cutoff of 70 Ry. The BLYP functional,[32,33] which gives good result in liquid water,[34,35] and the HO^-[25] description were used for all calculations. Standard norm-conserving fully separable[36] ab initio pseudopotentials of the Troullier−Martins[37] type were used for O and H.

Five simulations were conducted with 32 water molecules with one hydroxide anion and one hydrogen atom in a cubic box of 9.96 Å with periodic boundary conditions. One simulation was also performed containing 64 water molecules with one hydroxide anion and one hydrogen atom in a cubic box of 12.48 Å with periodic boundary conditions. The temperature was set to 330 K and controlled through a Nosé−Hoover thermostat.

The reaction mechanism will be shown to be complex with no simple reaction coordinate; however, for the last step of the reaction, formation of the new OH bond, the H−O distance can be naturally identified as the reaction coordinate (vide infra). Therefore, we have computed, for this last step, the free energy as a function of the OH distance. To do so we have employed the blue moon formalism[38] to compute the free energy gradient from constrained dynamics, at fixed OH distance. We have used 2 ps runs of 32 water molecules for each HO···H distance sampled. The constraint forces were measured only for the last ps.

To compute the histogram of encounter pairs life times, we performed a molecular dynamics (MD) simulation containing 512 water molecules, one hydroxide anion, and one H atom. The potentials used for this classical simulation were the same as the one used to prepare the CPMD run. These simulations, using an empirical force-field,[28] do not allow for proton transfer reactions but do respect global HO^- diffusion properties. The time step was 0.5 fs, and the simulation was performed in the NVT ensemble using a Nosé−Hoover thermostat at 300 K. After an equilibration of 500 ps the configurations were saved every 10 fs for 5 ns. We have performed 10 independent runs in order to average the needed statistical quantities. After the completion of the MD run, the distance between the H atom and the oxygen of the hydroxide anion was computed as a function of time step.

Figures 2, 3, and 5 where prepared using VMD.[39] Classical MD where done using Moldy.[40]

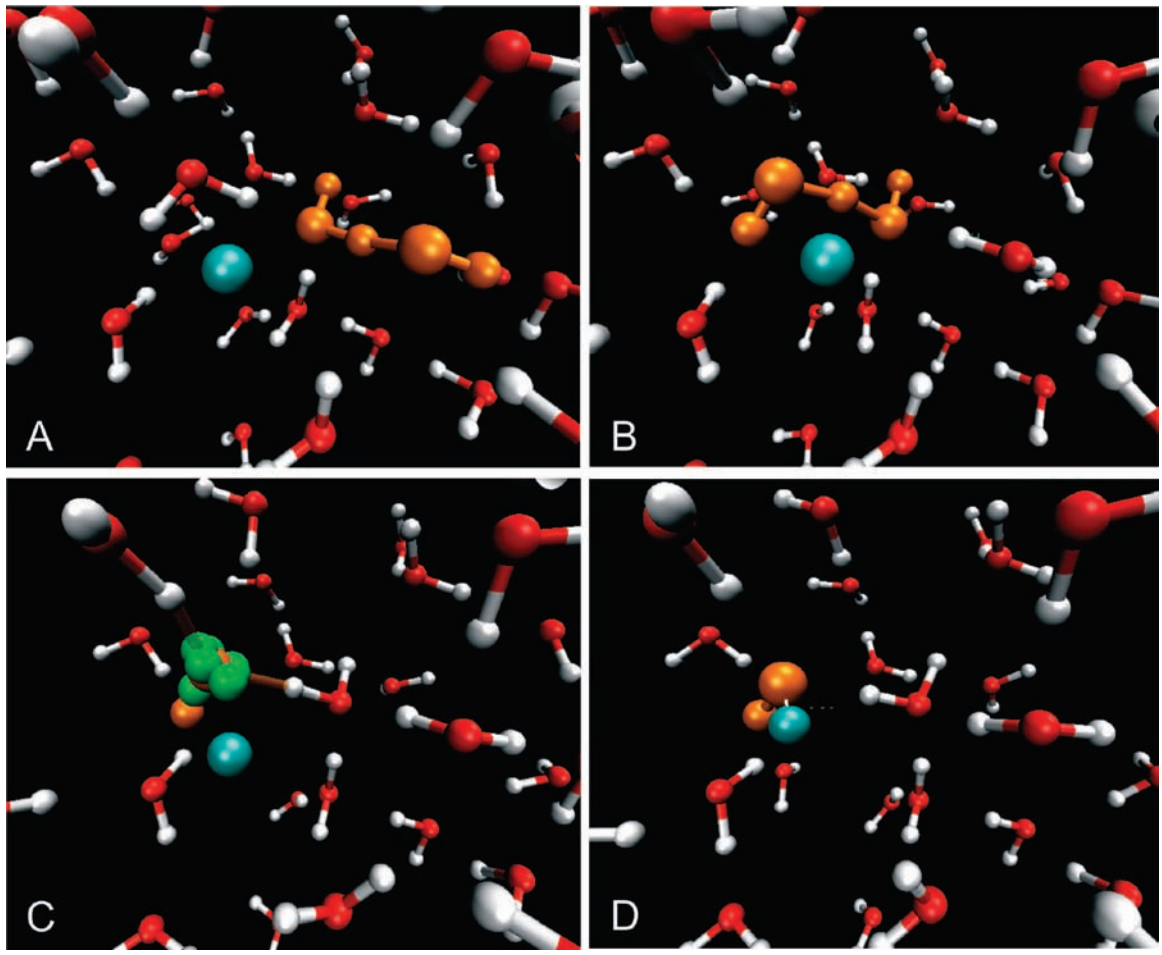

Figure 3. Snapshots of the reaction between the hydroxide anion and the H atom. (A) 80 fs before the reaction, the hydroxide anion is moving through the H bond network, leading to the formation of an extremely short-lived $H_3O_2^-$ supermolecule (in orange). (B) 60 fs before the reaction, the hydroxide anion is moving once more through the H bond network. (C): 40 fs before the reaction, the hydroxide anion is now ready to react with a lone pair pointing toward the H atom (plotted in green). (D): 0 fs after the reaction, a new water molecule is formed with an OH bond pointing toward the centre of the former H atom cavity.

Result and Discussion

Properties of the Reactant Prior to the Reaction. The hydroxide anion is strongly interacting with the water molecules of the liquid. Although its electronic structure has a C_∞ structure in vacuum, the result of the immersion in water dramatically change its electronic properties. From a quantitative point of view it may be seen, in our simulations, as a $OH^-(H_2O)_4$ cluster, as previously reported by Tuckerman et al.[41] Indeed, there is a high probability to find in the equatorial plane of the hydroxide anion four water molecules with an OH bond pointing toward the oxygen of the hydroxide anion. Therefore, all HO^- lone pairs are involved in H bonding. As pointed out elsewhere,[41] the hydroxide anion diffusive motion might be understood as a mix of diffusive motion and discrete jumping along the hydrogen bond network. In Figure S1 of the Supporting Information we have plotted, as a function of time, the squared displacement of the hydroxide anion. In between two jumps the hydroxide anion exhibits a remarkably stable solvation structure. The introduction of the $H^\bullet$ atom in the close vicinity of the hydroxide anion does not alter the picture of the isolated hydroxide anion as depicted by Tuckerman et al.[41]

The results of Kirchner et al. concerning the $H^\bullet$ atom motion in water[20] are also verified in the present work. The H atom is found to occupy a void of the liquid and does not polarize it. It is bouncing on the "wall" of the cavity and might move from void to void that are induced by the fluctuations of the H bond network of liquid water. The solvation structure of the $H^\bullet$ atom is explained by its localization in a void of the liquid. The surrounding water molecules do not exhibit any peculiar interactions except repulsion, that is, the electron of the $H^\bullet$ atom is not correlated to any of the ones of the liquid, and everything is happening as if the $H^\bullet$ atom was a hard sphere propagating in water (Figure S2, Supporting Information). This is in line with the fact that the spin density remains localized on the $H^\bullet$ atom throughout the simulation up to a few tens of femtosecond before the reaction studied here.

To summarize, both reactants do not significantly interact during the equilibration process up to a few tens of femtoseconds before the reaction and reveal properties that are in line with the precedent studies devoted to the hydroxide anion and the $H^\bullet$ atom in water.

Description of the Reaction. A reactive event was observed in all trajectories, occurring between 1 and 15 ps. This result is by itself surprising considering that the kinetic constant of reaction A is small (1.1×10^8 dm^3 mol^{-1} s^{-1}).[14] With reactant concentrations about 1 mol dm^{-3}, one expects a reaction time over the nanosecond that is beyond CPMD capabilities. A possible explanation would be an underestimation of the activation energy arising from an intrinsic limitation of DFT description, even though finite size effect on the water electronic structure can not be excluded.[23] Approximate exchange and correlation functionals fail to exactly cancel the self-interaction

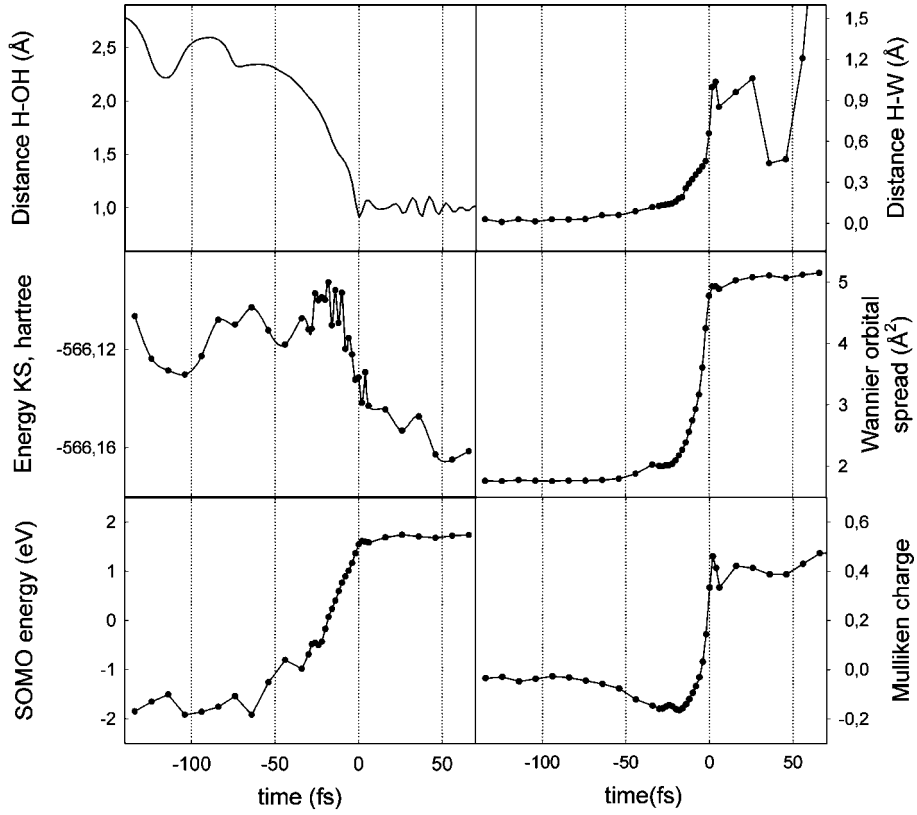

Figure 4. Evolution of the main energetic, orbital, and geometric data along the reaction path: (A) distance between the H proton and the oxygen where it will finally be bonded to, (B) the Kohn−Sham energy of the system, (C) energy of the singly occupied molecular orbital, (D) distance between the H proton and the Wannier center of the unpaired electron, (E) spread of the Wannier orbital of the unpaired electron, and (F) Mulliken charge on the H atom.

that is present in the Coulomb term, leading to the so-called self-interaction-error[42,43,18] This is more important for odd electron systems. However, by parametrization, BLYP is nearly self-interaction free for the hydrogen atom, and it has been shown to lead to a reasonable description of the solvated electron.[22]

Solvation and proton transfer properties of HO^- have also been shown to strongly depend on the functional used for the simulation[25] even though BLYP was suggested to be the better functional for such a description.[26]

It can also be suggested that a quantum description of hydrogen atom would be mandatory, but such a description (using, for example, path integral simulations) is expected to decrease the activation barriers.[41] However, we favor an alternative explanation: the periodicity of the system introduce a bias by increasing the encounter probability of the reactants. This "numerical confinement" effect is expected to significantly increase the reaction rate. This effect would be analogous to the well-known confinement effects on bimolecular kinetics formalized by Tachiya.[44]

Most of the simulation time is indeed used for the diffusion controlled encounter of the two reactive species. However, even after the two species have encountered (i.e., when a water molecule of the H cavity is also part of the hydroxide coordination sphere), the H can move in its cavity for hundreds of femtosecond before bonding to the hydroxide. We have plotted such a configuration in Figure 2. It has been extracted from the CPMD run 300 fs before the formation of the new water molecule (From now on, all time (τ) will be measured with respect to the water molecule formation.). Those nonreactive configurations live as long as the hydroxide anion possesses four H bonds in its equatorial plane. Indeed, in all the simulation we observed that the hydroxide anion has to make at least one jump (reaction B) by proton transfer though the H bond network before the reaction can occur.

$$HO^- \cdots H-OH \xrightarrow[H_2O]{} HO-H \cdots {}^-OH \qquad (B)$$

The four snapshots of Figure 3, recorded between $\tau = -100$ fs and $\tau = 0$ fs, depict a typical pathway from the nonreactive configuration shown in Figure 2 to a reactive configuration involving two proton jumps along the H bond network. As shown in Figure 3C, ($\tau = -50$ fs) the hydroxide is left undercoordinated and is directly part of the H atom cavity after the proton jumps. The new H−O bond is formed in 40 fs (Figure 3D). The hand explanation of such a reaction pathway is (i) the potentially reactive site of the hydroxide anion is obviously the oxygen; (ii) when the hydroxide anion is diffusing, it is H bonded to four water molecules in its equatorial plane; leaving no reactive site for the H atom; (iii) as a consequence of (i) and (ii) there is no lone pair available to form a new HO bond when the hydroxide anion has a diffusive motion. Therefore, a reactive configuration appears only after a proton transfer from a water molecule surrounding the H atom to the hydroxide anion occurs. This water molecule, whose HOH plane is usually tangential to the $H^\bullet$ atom cavity, has, after the proton transfer, a lone pair pointing toward the H atom cavity.

Figure 4A shows the time dependency of the distance between the H atom and the oxygen atom that will finally bind to it. Before $\tau = -40$ fs, the distance between the two nuclei exhibits a strong oscillatory nature associated with a "small" drift of the mean distance toward shorter ones (0.5 A per 100 fs). Between −40 and 0 fs, the oscillatory motions of the H atom

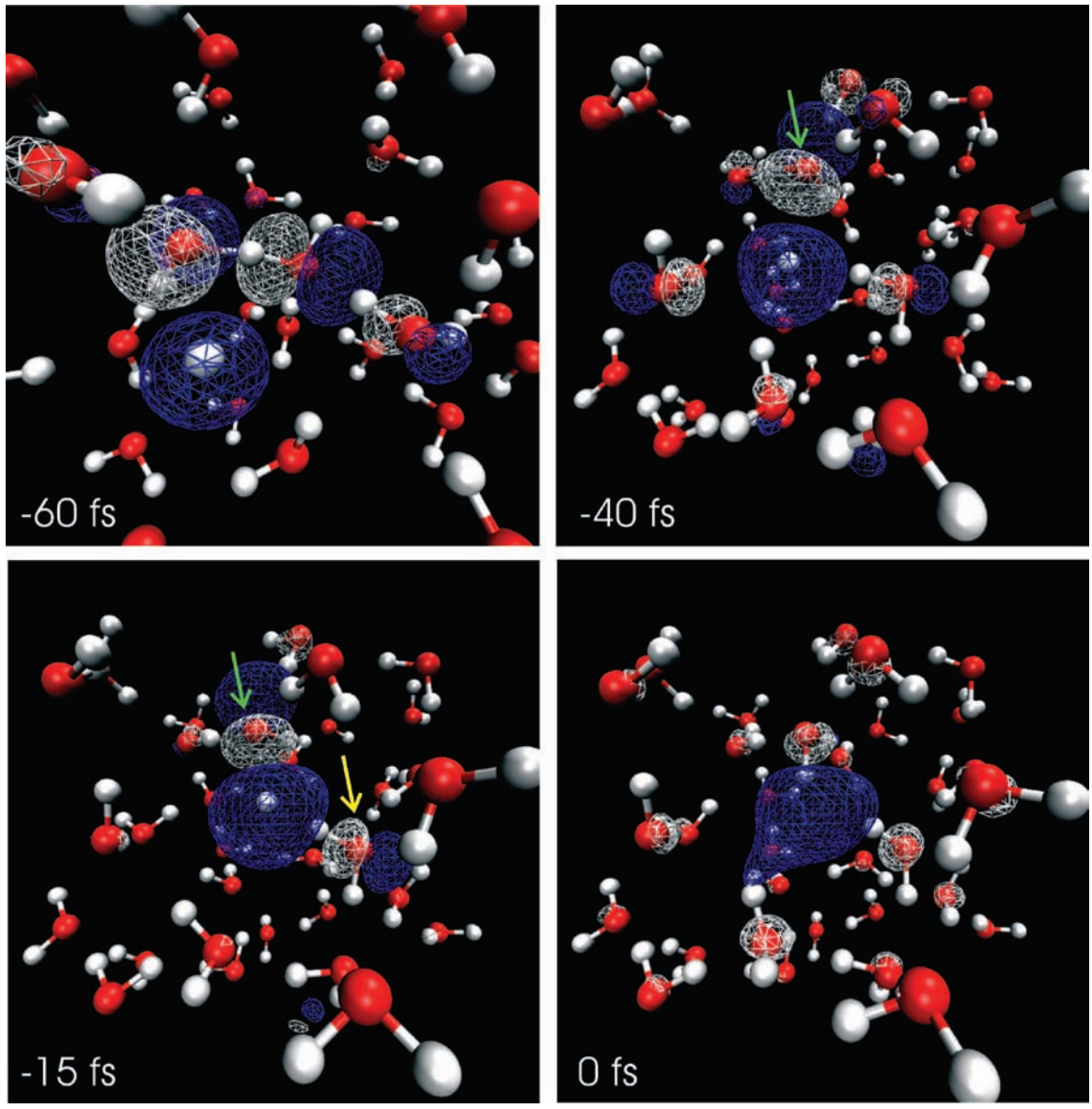

Figure 5. Evolution of the SOMO along the reaction path at different times before the formation of the new water molecule. Please note that for $\tau = -40$ and -15 fs, the HO^- is pointed at by a green arrow and that at $\tau = -15$ fs a yellow arrow shows the neighboring water molecule, referred to as NWM in the text.

are overdumped, and the distance between the nuclei is reducing extremely rapidly (over 1 A in less than 40 fs), the driving force of the reaction is now extremely high, and the two reactants react in a barrierless reaction. For positive time, the reaction is over, and the observed distance and oscillations are characteristic of a neutral water molecule.

To determine the nature of the reaction and of the intermediates, we have followed the evolution of the electronic structure during the reaction. Figure 4B shows the time dependency of the Kohn−Sham (KS) energy. That figure does not exhibit any peculiar feature up to a few femtoseconds before time zero. The KS energy then dramatically drops and exhibits a long time relaxation, up to a few tens of femtoseconds, after the reaction. That "slow" drift of the KS energy is due to the thermalization of the kinetic energy.

Figure 4C shows the evolution of the energy of the singly occupied molecular orbital (SOMO). Before the reaction, this orbital is evidently the one of the electron of the $H^\bullet$ atom, and after the reaction it is the one occupied by the excess electron. Interestingly, the SOMO KS energy is showing the same type of dependency than the nuclei distance: for times before -40 fs, the SOMO KS energy is "slowly" increasing but exhibits fluctuations; between -40 and 0 fs, the SOMO KS energy is increasing extremely fast. After time zero, the SOMO KS energy is extremely stable, demonstrating that the electronic properties of the products are already stabilized. The obvious antibonding character of the SOMO is then counterbalanced by the strong bonding character of H−O bond being formed and, as showed earlier, the total KS energy is dropping. The good correlation between the SOMO KS energy and the time dependency of the H−O distance demonstrates that this distance is a good candidate for being the principal coordinate of the reaction under study.

The main changes in the shape of the singly occupied KS orbital are pictured in Figure 5. At $\tau = -60$ fs, before the bond forming process starts, an orbital interaction between the H atom and the hydroxide already exist through the H-bonds network. Having an antibonding character, this interaction destabilizes this network and facilitates the proton transfer. The changes in shape of the SOMO after the proton transfers (Figure 5 $\tau =$

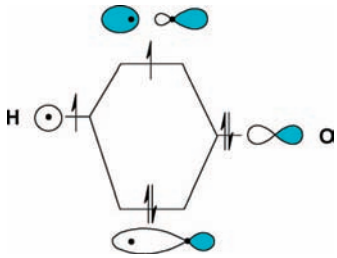

Figure 6. Molecular orbital scheme for the bond forming process.

−40, −15, and 0 fs) are in agreement with a bond formation process occurring by the simple overlap of the s orbital of the H atoms with a lone pair of the hydroxide (Figure 6). According to this interpretation, the unpaired electron is located at the end of the reaction in the newly formed H−O antibonding orbital. As seen in Figure 5 ($\tau = -40$, −15, and 0 fs), the main lobe of the SOMO is always pointing inside the cavity initially occupied by the H atom. The H nucleus progressively moves out of this lobe toward the hydroxide anion.

There is also, in all simulations, an overlap of the s orbital of the H atom with a H−O antibonding orbital (Figure 5, $\tau = -15$ fs) of a neighboring water molecule (NWM). This indicates that, even before the end of the bond formation process, the unpaired electron has recruited two water antibonding orbitals where to locate. These antibonding orbitals are reminiscent of the 2b2 MO of water, which has a strong directional character (p character).

The shape of the SOMO continues changing around $\tau = 0$ fs. It is still composed mainly of HO antibonding orbitals, but of a more diffuse type (with a s character on the oxygen atom, reminiscent of the 4a1 orbitals of free water, Figure 5). More water molecules are involved, and the SOMO spreads in the cavity initially occupied by the H atom. The solvation process is then, in the present case, rather a process of sharing an antibonding orbital on many water molecules rather than a process of digging a hole in which the electron will fall.

The SOMO suggests a progressive delocalization of the electron that can be more efficiently analyzed using the characteristics of its Wannier orbital.The distance with respect to the proton of the initial H atom and the spread of the Wannier center (W) corresponding to the unpaired electron are represented in Figure 4, panels D and E. Figure 4E shows that the delocalization of the unpaired electron and the H−O bond formation processes are grossly concomitant, so that at $\tau = 0$, the Wannier function of the unpaired electron has reached its final spread, that is, the electron hydration is completed. However, the evolution of H−W distance and of the Wannier spread remains moderate up to $\tau = -15$ fs, whereas the HO···H distance (Figure 4A) has already decreased to 1.5 A. As a consequence, a significant negative charge (−0.15 e) builds up on the H atom between −50 and −15 fs (Figure 6D). After $\tau = -15$ fs, the H−W distance increases suddenly while the Mulliken charge on the H atom becomes positive, as expected for an H atom in a water molecule. Therefore, we can assume that a H_2O^- anion transiently forms and subsequently releases its excess electron. After the HO bond formation ($\tau > 0$ fs), the Wannier center of the excess electron moves independently of its parent water molecule.

From −50 to 0 fs, the position of the Wannier center remains completely fixed with respect to the NWM observed in Figure 5 ($\tau = -15$ fs). Both the $W-H_{NWM}$ distance (1.96 ± 0.07A) and the $W-H_{NWM}-O_{NWM}$ angle (155 ± 7 °) are constant during the reaction process. These two facts confirm the stability of the interaction between the excess electron and NWM. Interestingly, the distance of $W-H_{NWM}$ is similar to the one between the center of mass of the aqueous electron and the nearest H atoms of its solvation sphere proposed by the model of Kevan[45] and the potential of Rossky et al.[46] We can consider that this neighboring water molecule facilitates the charge separation process by "pre-solvating" the excess electron.

As the result of the present work, we may propose that the solvation of an excess electron is its localization in H−O antibonding orbitals of the water molecules. This picture is supported by the recent study of Auger electron decay in water by Nordlund et al.[47] It implies also a coupling of the unpaired electron with the stretching modes of the water molecules involved in the "solvation". This coupling has indeed been demonstrated by the observation of an infrared[48,49] and of a Raman[50] spectrum of the hydrated electron.

From these observations we may propose also the following scheme C for the reaction between $H^\bullet$ and HO^-.

$$H^\bullet_{aq} + HO^-_{aq} \overset{\text{Diffusion in solution}}{\rightleftharpoons} (H^\bullet_{aq}, HO^-_{aq}) \qquad \text{(C1)}$$

$$(H^\bullet_{aq}, HO^-_{aq}) \overset{\text{H diffusion in its cavity}}{\rightleftharpoons} (H^\bullet, HO^-_{aq}) \qquad \text{(C2)}$$

$$(H^\bullet, HO^-_{aq}) \overset{\text{Proton transfer}}{\rightleftharpoons} (H^\bullet, HO^-)_{contact} \qquad \text{(C3)}$$

$$(H^\bullet, HO^-)_{contact} \rightarrow [(H_2O)^-]^{\neq} \rightarrow e^-_{aq} \qquad \text{(C4)}$$

As discussed previously, the diffusion process of the two species through the solution is not expected to be accurately described by the simulation (step C1) due to its finite size, but its end can be precisely defined by the time when a water molecule of the H cavity is also part of the hydroxide coordination sphere (that will be described hereafter as the formation of the encounter pair ($H^\bullet_{aq}$, HO^-_{aq})). The bond forming process itself starts at the formation of a contact pair between H and HO^-, (step C4). Between these two steps, which are separated in time by hundreds of fs, occurs a diffusion step of H inside its cavity (step C2), followed by a proton transfer step (step C3). This proton transfer opens the coordination of the hydroxide and allows the formation of the contact pair and the subsequent bond formation process to occur. We must also notice that there is no formation of an H_2O^- as a long-lived intermediate.

Finally, we would like to address the question of how such a scheme can be of any help to understand the poor reactivity of the H atom compared to other radiolytic species. Therefore, we tried to evaluate the activation energy associated to the various steps described above.

For the bond forming step (step C4), the H−O distance can be naturally identified as the reaction coordinate. Therefore, we conducted constrained molecular dynamics along this reaction coordinates. According to the blue moon ensemble formalism,[38] the value of the constraint gives straightforward access to the free energy value.

The evolution of the free energy as a function of the proposed reaction coordinates is shown in Figure 7. A maximum in free energy is located at 1.8 Å, a bond length below which the reaction is expected to spontaneously evolve toward the solvated electron formation. The electron is completely and irreversibly

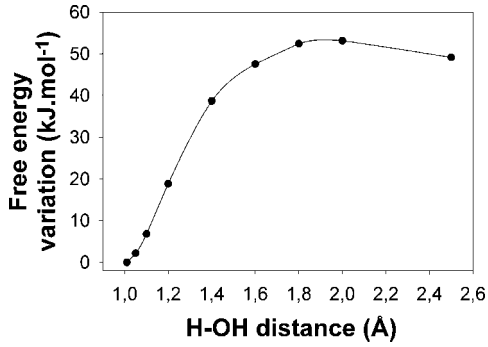

Figure 7. Evolution of the free energy along the reaction coordinate defined as the H···OH distance.

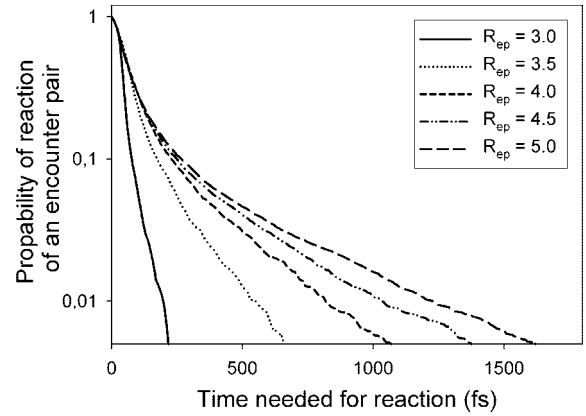

Figure 8. Evolution of the encounter pair reaction probability as a function of the time needed for the reaction (τ). The evolution of the reaction probability is showed for five different values of the encounter pair distance formation R_{ep} (see text) from 5 to 3 Å.

released from the H atom for an O−H length smaller than 1.3 Å. For the backward reaction $[e^-_{aq} \rightarrow (H^\bullet, HO^-)_{contact}]$, the barrier for the electron attachment to a water molecule is thus evaluated to 50 kJ/mol according to Figure 7. This value compares well to the experimental value,[14] which of course does not prove that the electron attachment to a distorted water molecule, as studied here, is the sole pathway for this reaction. On the other hand, for the forward reaction (C4), the activation barrier is only of a few kJ/mol and cannot explain the poor reactivity of the H atom. Indeed, in all simulation this step occurs in less than 50 fs.

Step C4 is obviously not the rate limiting step, and we tried to determine the activation energy associated with the preceding steps C3 and C2 (C1 is a diffusion step that can not determine the activation barrier for the reaction).

For the proton transfer step (C3), the activation energy for hydroxide mobility across the H bond network was evaluated to be 12 kJ mol^{-1}.[41,51] This proton transfer is also accompanied by the loss of one H-bond around OH^-.

For the "in cavity" diffusion process (step C2) we can get a rough estimation of the translational entropy loss associated with the evolution from a free H atom in its cavity to a H atom immobilized at a border of the cavity using a Sackur−Tetrode formula (eq D), modified for liquids;[52]

$$S_{tr} = R\left(\ln\frac{v_f}{\Lambda^3} + \frac{5}{2}\right) \qquad \text{(D)}$$

where R is the gas constant, Λ is the thermal de Broglie wavelength of the H atom, and v_f is the free volume in which the hydrogen can move inside the cavity.

Taking into account the oxygen and hydrogen radial distribution function of water around the H atom determined by Kirchner et al.,[20,53] a simple estimate for the free volume would be a spherical cavity of 2.0 Å radius with impenetrable walls. With these assumptions we get a variation of $T\,S_{tr}$ greater than 15 kJ mol^{-1} prior to the proton transfer.

This means that the two processes (C2 and C3) leading to the formation of a contact pair prior to the covalent bond formation would require an overall activation free energy of about 27 kJ mol^{-1}. Considering that the total activation free energy determined by Bartels et al. is 31 kJ.mol^{-1}, we can then propose that the steps C2 and C3 are the critical ones in determining the H atom reaction rate. Indeed, in all simulations, these processes took between 500 fs and 1 ps; although this may indicate that the time scale with DFT based FPMD is too short, it shows that these steps are the critical ones in our simulations.

To explain the very small reactivity of the H atom, we postulate that the steps C2 and C3 create a lag time in the reaction dynamics. To understand the potential impact of this lag time on the reaction, we performed extensive classical molecular dynamics simulations. The aim was to know the proportion of diffusive encounters between the HO^- and the cavity surrounding the H atom that last long enough to allow a reaction to occur.

If we assume, for a characteristic time of the reaction (τ), that an encounter pair (defined as an H atom and an hydroxide anion being closer than a given distance R_{EP}) being continuously formed for a time t has a probability of having reacted at that time to be $p(t,\tau)$, we can then define that probability $P_{EP}(\tau)$ that an encounter pair reacts with eq E,

$$P_{EP}(\tau) = \frac{\int_0^\infty p(t,\tau) \times \mathrm{histo}_{R_{EP}}(t)\,\mathrm{d}t}{\int_0^\infty \mathrm{histo}_{R_{EP}}(t)\,\mathrm{d}t} \qquad \text{(E)}$$

where $\mathrm{histo}_{R_{EP}}(t)$ is the histogram of the live time of the encounter pairs based on diffusion only, for a given value of the encounter pair formation distance (R_{EP}). We must notice that employing classical MD to compute $\mathrm{histo}_{R_{EP}}(t)$ and P_{EP} allows us to incorporate non-Markovian aspects of the dynamics of OH^- in the surroundings of the H atom, at the time scales considered.[54] To test the lag time hypotheses, $p(t,\tau)$ was chosen to be a Heaviside function of t starting at the lag time (τ). $P_{EP}(\tau)$ is presented in Figure 8 as a function of (τ), for different values of the distance (R_{EP}). From the CPMD simulations, we estimated R_{EP} to be 4 Å (below this value, a water molecule of the H cavity is also part of the hydroxide coordination sphere) and τ to be 800 fs. According to Figure 8, with these two values only 1% of the diffusive encounters last long enough to allow a reaction to occur. For water we then expect a reaction rate roughly 100 times smaller than the diffusion limit, that is, 10^8 dm^3 mol^{-1} s^{-1}. The latter value compares well with the experimental one.[14]

Conclusion

FPMD of the reaction between the H atom and the hydroxide anion reveals a complex mechanism, controlled by proton transfers in the coordination sphere of the hydroxide and by the diffusion of the H atom in its cavity. The hydrated electron production mechanism reveals the key role of water antibonding orbitals in the solvation process. The extremely small reactivity

of the H atom compared to other species like OH is explained by the existence of a lag time between the encounter pair formation and the reaction due to its diffusion in the cavity. The coupling between CPMD and MD runs enables us to evaluate the impact of this lag time on the reaction rate in liquid phase. This study demonstrates the capability of FPMD to decipher unknown mechanism without any a priori.

Supporting Information Available: Figure S1, square displacement of the hydroxide anion along a single trajectory; and Figure S2, square displacement of the H atom along a single trajectory. This material is available free of charge via the Internet at http://pubs.acs.org.

References and Notes

(1) Rotureau, P.; Renault, J. P.; Lebeau, B.; Patarin, J.; Mialocq, J. C. *ChemPhysChem* **2005**, *6*, 1316–1323.
(2) Molin, M.; Renault, J.-P.; Lagniel, G.; Pin, S.; Toledano, M.; Labarre, J. *Free Radical Biol. Med.* **2007**, *43*, 136–144.
(3) Jaeger, C. D.; Bard, A. J. *J. Phys. Chem.* **1979**, *83*, 3146–3152.
(4) Ohsawa, I.; Ishikawa, M.; Takahashi, K.; Watanabe, M.; Nishimaki, K.; Yamagata, K.; Katsura, K.-i.; Katayama, Y.; Asoh, S.; Ohta, S. 2007, *13*, 688−694.
(5) Czapski, G.; Stein, G. *Nature* **1958**, *182*, 598–598.
(6) Shiraishi, H.; Sunaryo, G. R.; Ishigure, K. *J. Phys. Chem.* **1994**, *98*, 5164–5173.
(7) Mezyk, S. P.; Bartels, D. M. *J. Phys. Chem. A* **2005**, *109*, 11823–11827.
(8) Ye, M. Y.; Madden, K. P.; Fessenden, R. W.; Schuler, R. H. *J. Phys. Chem.* **1986**, *90*, 5397–5399.
(9) Deeble, D. J.; Parsons, B. J.; Johnson, G. R. A. *Radiat. Phys. Chem.* **1990**, *36*, 487–491.
(10) Draganic, Z. D.; Draganic, I. G. *J. Phys. Chem.* **1972**, *76*, 2733–&
(11) Bartels, D. M.; Mezyk, S. P. *J. Phys. Chem.* **1993**, *97*, 4101–4105.
(12) Cline, J.; Takahashi, K.; Marin, T. W.; Jonah, C. D.; Bartels, D. M. *J. Phys. Chem. A* **2002**, *106*, 12260–12269.
(13) Jortner, J.; Rabani, J. *J. Am. Chem. Soc* **1961**, *83*, 4868–&
(14) Han, P.; Bartels, D. M. *J. Phys. Chem.* **1992**, *96*, 4899–4906.
(15) Han, P.; Bartels, D. M. *J. Phys. Chem.* **1990**, *94*, 7294–7299.
(16) Marin, T. W.; Jonah, C. D.; Bartels, D. M. *J. Phys. Chem. A* **2005**, *109*, 1843–1848.
(17) Hart, E. J.; Anbar, M. *The Hydrated Electron*; Wiley-Interscience: New York, 1970.
(18) VandeVondele, J.; Sprik, M. *Phys. Chem. Chem. Phys.* **2005**, *7*, 1363–1367.
(19) Gaigeot, M. P.; Vuilleumier, R.; Stia, C.; Galassi, M. E.; Rivarola, R.; Gervais, B.; Politis, M. F. *J. Phys. B: At., Mol. Opt. Phys.* **2007**, *40*, 1–12.
(20) Kirchner, B.; Stubbs, J.; Marx, D. *Phys. Rev. Lett.* **2002**, 89.
(21) Park, I.; Cho, K.; Lee, S.; Kim, K. S.; Joannopoulos, J. D. *Comput. Mater. Sci.* **2001**, *21*, 291–300.
(22) Boero, M.; Parrinello, M.; Terakura, K.; Ikeshoji, T.; Liew, C. C. *Phys. Rev. Lett.* **2003**, 90.
(23) Prendergast, D.; Grossman, J. C.; Galli, G. *J. Chem. Phys.* **2005**, 123.
(24) Boero, M. *J. Phys. Chem. A* **2007**, *111*, 12248–12256.
(25) Tuckerman, M. E.; Chandra, A.; Marx, D. *Acc. Chem. Res.* **2006**, *39*, 151–158.
(26) Chandra, A.; Tuckerman, M. E.; Marx, D. *Phys. Rev. Lett.* **2007**, *99*, 145901.
(27) Berendsen, H. J. C.; Grigera, J. R.; Straatsma, T. P. *J. Phys. Chem.* **1987**, *91*, 6269–6271.
(28) Guissani, Y.; Guillot, B.; Bratos, S. *J. Chem. Phys.* **1988**, *88*, 5850–5856.
(29) Gai, H.; Garrett, B. C. *J. Phys. Chem.* **1994**, *98*, 9642–9648.
(30) Car, R.; Parrinello, M. *Phys. Rev. Lett.* **1985**, *55*, 2471–2474.
(31) CPMD, v 3.9.1; Festkorperforschung Stuttgart and IBM Zurich Research Laboratory, 2004. Available at http://www.cpmd.org.
(32) Becke, A. D. *Phys. Rev. A* **1988**, *38*, 3098 LP–3100.
(33) Lee, C.; Yang, W.; Parr, R. G. *Phys. Rev. B* **1988**, *37*, 785 LP–789.
(34) Sprik, M.; Hutter, J.; Parrinello, M. *J. Chem. Phys.* **1996**, *105*, 1142–1152.
(35) Grossman, J. C.; Schwegler, E.; Draeger, E. W.; Gygi, F.; Galli, G. *J. Chem. Phys.* **2004**, *120*, 300–311.
(36) Kleinman, L.; Bylander, D. M. *Phys. Rev. Lett.* **1982**, *48*, 1425 LP–1428.
(37) Troullier, N.; Martins, J. L. *Phys. Rev. B* **1991**, *43*, 1993 LP–2006.
(38) Sprik, M.; Ciccotti, G. *J. Chem. Phys.* **1998**, *109*, 7737–7744.
(39) Humphrey, W.; Dalke, A.; Schulten, K. *J. Mol. Graph.* **1996**, *14*, 33–&
(40) Refson, K. *Comput. Phys. Commun.* **2000**, *126*, 310–329.
(41) Tuckerman, M. E.; Marx, D.; Parrinello, M. *Nature* **2002**, *417*, 925–929.
(42) Perdew, J. P.; Zunger, A. *Phys. Rev. B* **1981**, *23*, 5048–5079.
(43) Zhang, Y. K.; Yang, W. T. *J. Chem. Phys.* **1998**, *109*, 2604–2608.
(44) Tachiya, M. In *Kinetics of Nonhomogeneous Processes. A Practical Introduction for Chemists, Biologists, Physicists, and Material Scientists*; Freeman, G. R., Ed.; Wiley: New York, 1987; pp 575−650.
(45) Kevan, L. *Radiat. Phys. Chem.* **1981**, *17*, 413–423.
(46) Schnitker, J.; Rossky, P. J. *J. Chem. Phys.* **1987**, *86*, 3462–3470.
(47) Nordlund, D.; Ogasawara, H.; Bluhm, H.; Takahashi, O.; Odelius, M.; Nagasono, M.; Pettersson, L. G. M.; Nilsson, A. *Phys. Rev. Lett.* **2007**, 99.
(48) Hammer, N. I.; Shin, J. W.; Headrick, J. M.; Diken, E. G.; Roscioli, J. R.; Weddle, G. H.; Johnson, M. A. *Science* **2004**, *306*, 675–679.
(49) Thaller, A.; Laenen, R.; Laubereau, A. *Chem. Phys. Lett.* **2004**, *398*, 459–465.
(50) Tauber, M. J.; Mathies, R. A. *J. Phys. Chem. A* **2001**, *105*, 10952–10960.
(51) Agmon, N. *Chem. Phys. Lett.* **2000**, *319*, 247–252.
(52) Amzel, L. M. *Proteins: Struct., Funct., Genet.* **1997**, *28*, 144–149.
(53) Kirchner, B.; Hutter, J.; Kuo, I. F. W.; Mundy, C. J. *Int. J. Mod. Phys. B* **2004**, *18*, 1951–1962.
(54) If the function $\text{histo}_{R_{EP}}(t)$ would be simply an exponential with a characteristic time τD governed by the mutual diffusion constant D of the pair, and $p(t,\tau R)$ also be an exponential arising from a constant probability of reaction per unit time $dt/\tau R$, one would obtain a probability $EP = \tau D/(\tau R + \tau D)$, in agreement with the classical reaction rate theory.

JP800269S